# Excitation of coupled phononic frequency combs via two-mode parametric three-wave mixing

Adarsh Ganesan, Cuong Do, and Ashwin Seshia*
*Nanoscience Centre, University of Cambridge, Cambridge, United Kingdom*

(Received 12 October 2017; published 3 January 2018)

This paper builds on the recent demonstration of three-wave mixing based phononic frequency comb. Here, in this process, an intrinsic coupling between the drive and resonant frequency leads to a frequency comb of spacing corresponding to the separation between drive and resonant frequency. In this paper, through the coupling with other identical devices, we demonstrate the emergence of two different frequency comb regimes using a single tone external drive signal. Several interesting features for coupled frequency combs are identified, including the following: (1) the spacing of the component frequency combs are controlled by two different resonant frequencies, each associated with two different modes; (2) the nonlinear drive level dependence is different for the component frequency combs; (3) mutually exclusive well-bounded regimes for each component frequency comb exist, and such regimes are not merely described by well-known parametric resonance thresholds.

DOI: 10.1103/PhysRevB.97.014302

This paper builds upon the recent experimental demonstration of the phononic counterpart of optical frequency combs in a micromechanical vibratory device [1]. The generation of these phononic frequency combs is described by a nonlinear three-wave mixing process, as theoretically outlined in Ref. [2]. Through this pathway, a single drive tone results in the generation of equidistant and phase-coherent spectral lines corresponding to the frequency comb. The spacing between these spectral lines corresponds to the separation between the drive and resonant frequency of a primary eigenmode. While this phenomenon displays some similarity to the well-known parametric resonance [3–11] in terms of the self-excitation of modes, properties exist that are unique to phononic frequency combs viz. (1) an array of equidistant spectral lines are generated for a single tone drive excitation; (2) a very specific range of drive frequencies is required for their excitation; and (3) the comb spacing is controlled by an eigenmode's natural frequency.

In addition to the intriguing traits of phononic frequency combs, it should be noted that the effects are evidenced in an accessible experimental testbed (a well-established free-free beam mechanical device [12–17]) under ambient conditions, facilitating the ease of further experimental studies and practical application. Building on the initial demonstration [1], this paper demonstrates that it is possible to engineer devices operating in multiple frequency comb regimes by coupling multiple free-free beam structures together. In such a configuration, closely spaced eigenmodes with similar characteristics can be driven by the same external drive tone. When the frequency of this drive tone is in the vicinity of the natural frequencies of multiple eigenmodes, the resulting response is dominated by a specific eigenmode, depending on the drive frequency. As a result, multiple frequency combs with spacing determined by the difference in the frequency of the drive tone and the predominantly driven eigenmode can be expected. The resulting richness in dynamical behavior, evidenced by coupling, explored in this paper is notionally analogous to previous studies exploring coupling in nonlinear micromechanical and nanomechanical resonators and oscillators to illustrate emergent effects (see, e.g., in Fig. 4 of Ref. [18] and Fig. 8 of Ref. [19], among others [20–32]).

For this experimental study, a system of two-coupled Si-based micromechanical free-free beam structures of dimensions 1100 $\mu$m × 350 $\mu$m × 11 $\mu$m is considered. The mechanical coupler is a beam of dimensions 20 $\mu$m × 2 $\mu$m × 11 $\mu$m and links the two free-free beam structures at the midpoint [Fig. 1(a)]. The device also consists of the 0.5-$\mu$m-thick AlN and 1-$\mu$m-thick Al layers deposited on the Si surface for piezoelectric actuation. To preserve the uniformity, the AlN and Al patterns of the two free-free beam microstructures are identical. The length extensional modes associated with this resonant device are driven by an external drive signal, following from previous experimental results where phononic frequency combs are generated by driving length-extensional modes [1,33–36]. However, since this paper utilizes a system of two-coupled free-free beams, there are correspondingly two fundamental length-extensional mode solutions (Supplemental Material Figs. S1-D and S1-E [37]), one of which represents the out-of-phase motion (Supplemental Material Fig. S1-D [37]) of two beams and the other represents the in-phase case (Supplemental Material Fig. S1-E [37]). To drive these modes, the signal derived from Agilent 335ARB1U is applied to Al electrodes patterned on both the beams, and the resulting electrical response corresponding to the mechanical motion of the device is probed using Agilent Infiniium 54830B DSO. For the independent validation, the out-of-plane component of the resonant motion of the device is also monitored using a laser Doppler vibrometer (LDV).

Figure 1(b) shows the output spectrum when an electrical signal of $S_{\text{in}}(f_d = 3.86\,\text{MHz}) = 23$ dBm is applied. In this figure, two thick spectral features closer to $f_d$ and $\frac{f_d}{2}$ exist. The zoomed-in views indicate the correspondence of these features to the frequency combs. To explore these frequency combs further, the experiments were carried out at wide-ranging drive

*Corresponding author: aas41@cam.ac.uk

 

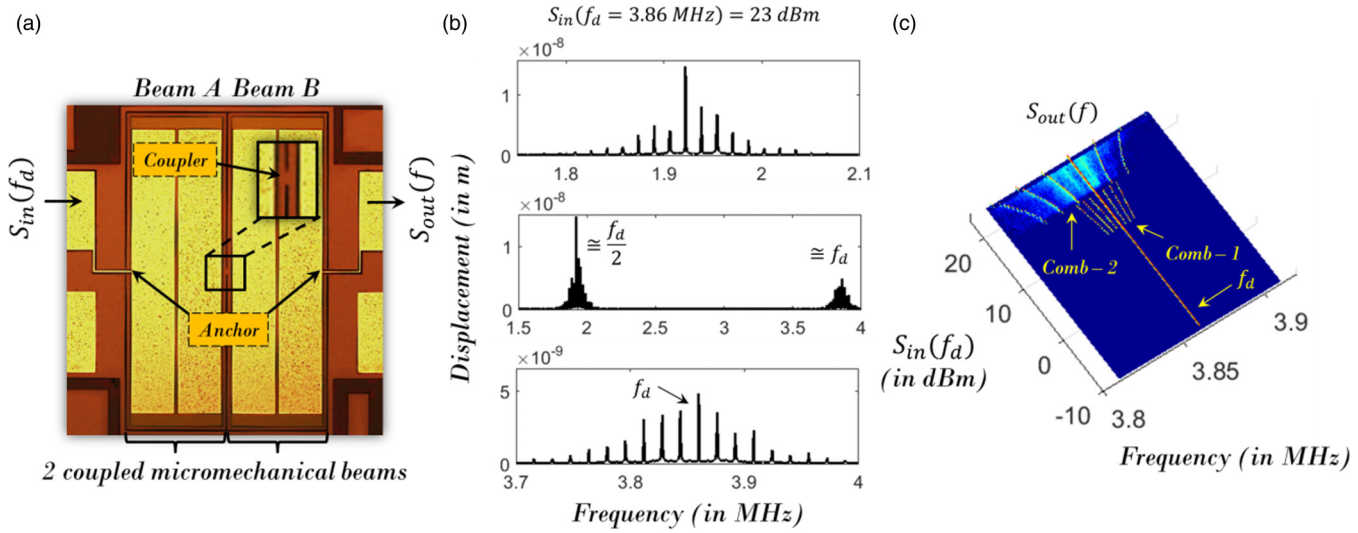


FIG. 1. Observation of coupled phononic frequency combs via two-mode three-wave mixing. (a) An electrical signal $S_{\text{in}}(f_d = 3.86\ \text{MHz})$ is applied on a mechanically coupled free-free beam microstructure. (b) The frequency spectrum of the vibrational response for $S_{\text{in}}(f_d = 3.86\ \text{MHz}) = 23$ dBm (measured using laser Doppler vibrometer). Top: The zoomed-in view of the spectrum around $f_d/2$. Middle: The zoomed-out view. Bottom: The zoomed-in view of the spectrum around $f_d$. (c) The spectral maps of the output electrical signal $S_{\text{out}}$ for different drive conditions $S_{\text{in}}(f_d = 3.86\ \text{MHz}) = -10$ to 23.5 dBm (measured using electrical spectrum analyser).

power levels for the same drive frequency $f_d = 3.86$ MHz. The electrical spectra $S_{\text{out}}$ for $S_{\text{in}}(f_d = 3.86\ \text{MHz})$, ranging from $-10$ dBm to 23.5 dBm, are presented in the condensed Fig. 1(c). For drive levels below 10 dBm, only the drive tone is observed. However, further increase in $S_{\text{in}}$ leads to a frequency comb. It is now surprising to note the drastic shift in the spacing of the frequency comb above the critical $S^*_{\text{in}} = 16.5$ dBm. In order to conclude whether this observed shift corresponds to an auxiliary nonlinear pathway associated with the generation of the same frequency comb 1 or results from the transition to a different frequency comb altogether, the nature of the frequency combs around the parametrically excited subharmonic tone is investigated.

At a low drive level of $-5$ dBm, parametric resonance is absent. Hence, only the drive tone is observed [Fig. 2(a)]. However, when the drive level is further increased to 5 dBm, in addition to the drive tone, there is also an excitation of a subharmonic tone corresponding to the parametric resonance [Fig. 2(b)]. Despite parametric excitation, frequency combs are not formed at this drive condition. However, for the drive levels 15 dBm and 23 dBm, both the frequency combs and parametric resonance are observed [Figs. 2(c) and 2(d)]. The different drive power level thresholds associated with the parametric resonance and frequency combs indicate that parametric resonance is only a necessary but not sufficient condition for frequency comb formation. Figures 2(c) and 2(d) also present interesting qualitative differences in the frequency combs formed at the drive levels 15 dBm and 23 dBm. While the tone $\frac{f_d}{2}$ is observed in the frequency combs at 15 dBm, such a tone is absent at 23 dBm. Hence, in addition to the increased frequency spacing of combs at 23 dBm, as compared to those at 15 dBm, there is also a fundamental difference in the nature of these combs. So, the observed drastic frequency shift above the critical $S^*_{\text{in}} = 16.5$ in Fig. 1(c) cannot simply be due to an additional nonlinear process associated with the generation of the same frequency comb. However, it has to be explained by the transition from one class of frequency combs to another. Such classes of frequency combs can be qualitatively described by $f_d \pm n(f_d - \tilde{f}_1)$; $\frac{f_d}{2} \pm n(f_d - \tilde{f}_1)$ and $f_d \pm n(f_d - \tilde{f}_2)$; $\frac{\tilde{f}_2}{2} \pm n(f_d - \tilde{f}_2)$, respectively. Here, $\tilde{f}_1$ and $\tilde{f}_2$ correspond to the two different re-normalized resonant frequencies.

To understand these experimental observations in the context of previous demonstration of frequency comb in Ref. [1], the following dynamical model is considered:

$$\ddot{Q}_i = -\omega_i^2 Q_i - 2\zeta_i \omega_i \dot{Q}_i + \sum_{\tau_1=1}^{2}\sum_{\tau_2=1}^{2} \alpha_{\tau_1\tau_2} Q_{\tau_1} Q_{\tau_2} + \sum_{\tau_1=1}^{2}\sum_{\tau_2=1}^{2}\sum_{\tau_3=1}^{2} \beta_{\tau_1\tau_2\tau_3} Q_{\tau_1} Q_{\tau_2} Q_{\tau_3} + P\cos(\omega_d t), \quad (1)$$

where $P$ is the drive level, $\alpha$ and $\beta$ are quadratic coupling coefficients, and $\omega_{i=1,2}$ and $\zeta_{i=1,2}$ are natural frequencies and damping coefficients of modes $i = 1, 2$ respectively.

Here, when this coupled system of two modes is driven closer to $\omega_1$, mode 1 dominates the response. With an increased power level $P$, the modal displacement $Q_1$ may also get high enough to trigger parametric excitation of mode 2 through the $Q_1 Q_2$ nonlinearity. Such parametrically excited tone is expected to have a frequency $\frac{\omega_d}{2}$ and is closer to the resonant frequency of mode 2: $\omega_2$. However, the recent experiments on the two-mode three-wave mixing based frequency comb [1] have indicated the possibility for $\frac{\omega_1}{2}$ excitation instead of $\frac{\omega_d}{2}$. This particularly occurred when $\omega_d$ is set outside the dispersion band, i.e., $|\omega_d - \omega_1| > \delta$. Once the parametric excitation of $\frac{\omega_1}{2}$ is introduced, the frequency combs $\omega_d \pm n(\omega_d - \omega_1)$; $\frac{\omega_1}{2} \pm n(\omega_d - \omega_1)$ are generated through the high-order nonlinear

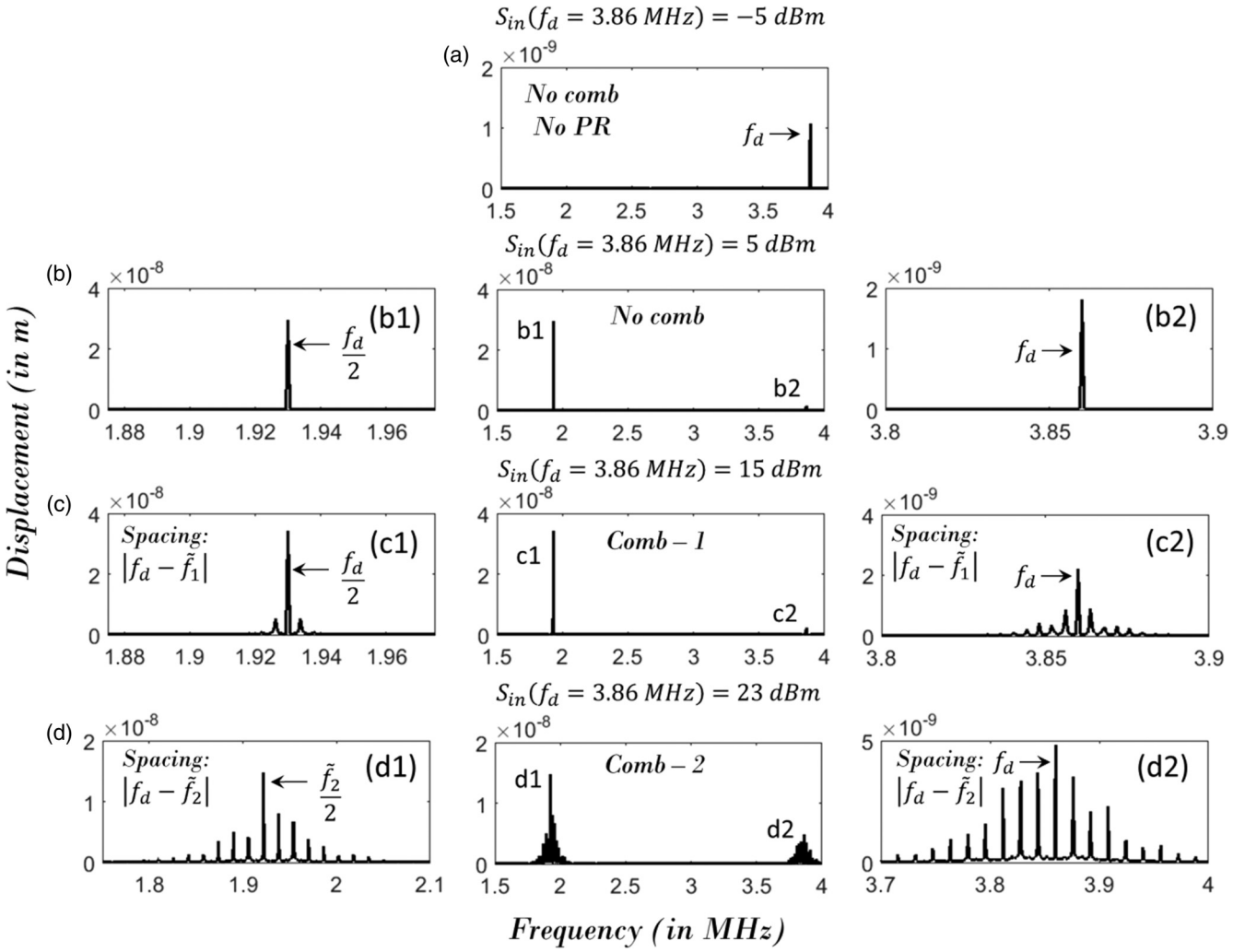


FIG. 2. Observation of coupled phononic frequency combs via two-mode three-wave mixing. (a)–(d) The frequency spectra of the vibrational response for $S_{\text{in}}(f_d = 3.86\ \text{MHz}) = -5$, 5, 15, and 23 dBm, respectively (measured using laser Doppler vibrometry). (b1), (c1), and (d1) The zoomed-in views of the spectra (b), (c), and (d) around $f_d/2$, respectively. (b2), (c2), and (d2) The zoomed-in views of the spectra (b), (c), and (d) around $f_d$, respectively.

mixing processes.

$$\ddot{Q}_i = -\omega_i^2 Q_i - 2\zeta_i \omega_i \dot{Q}_i + \sum_{\tau_1=1}^{3}\sum_{\tau_2=1}^{3} \alpha_{\tau_1\tau_2} Q_{\tau_1} Q_{\tau_2} + \sum_{\tau_1=1}^{3}\sum_{\tau_2=1}^{3}\sum_{\tau_3=1}^{3} \beta_{\tau_1\tau_2\tau_3} Q_{\tau_1} Q_{\tau_2} Q_{\tau_3} + P\cos(\omega_d t); \quad i = 1,2,3. \tag{2}$$

Now, we turn to a system of three coupled modes, and the modified dynamics is presented in Eq. (2). Let us consider the case where the drive frequency $\omega_d$ is simultaneously closer to the resonant frequencies of two modes: $\omega_1$ and $\omega_2$ (Supplemental Material Fig. S1 [37]). Further, $\omega_d$ is also closer to twice the resonant frequency of a third mode $\omega_3$. In this case, modes 1 and 2 are directly excited at first. For high drive power levels of $P$, the modal displacements $Q_1$ and $Q_2$ may also achieve sufficiently high values to also independently parametrically excite mode 3 through $Q_1Q_3$ and $Q_2Q_3$ nonlinearities. Based on the current understanding, the frequency of this tone is expected to be $\frac{\omega_d}{2}$. However, due to the nonlinear three-wave mixing processes, deviations from this frequency may also be encountered similar to the case presented before. While such deviations are possible through the dynamical Eq. (2), as demonstrated numerically in Ref. [2], the analytics describing them as a function of the various system parameters are not yet well defined. Qualitatively, since $\omega_d$ is closer to both $\omega_1$ and $\omega_2$, the parametric excitation of tones at either $\frac{\omega_1}{2}$ or $\frac{\omega_2}{2}$ or even $\frac{\omega_d}{2}$ may be possible. Following the excitation of $\frac{\omega_1}{2}$ or $\frac{\omega_2}{2}$, the high-order mixing may result in the frequency combs $\omega_d \pm n(\omega_d - \omega_1)$; $\frac{\omega_1}{2} \pm n(\omega_d - \omega_1)$ or $\omega_d \pm n(\omega_d - \omega_2)$; $\frac{\omega_2}{2} \pm n(\omega_d - \omega_2)$, respectively. In contrast, when $\frac{\omega_d}{2}$ is excited, we may not expect a frequency comb based on our current understanding of frequency comb; however, our experiments show otherwise. That is, the frequency combs $\omega_d \pm n(\omega_d - \omega_2)$; $\frac{\omega_d}{2} \pm n(\omega_d - \omega_2)$ are observed at certain drive conditions [Fig. 2(b)]. To explain the emergence of such frequency combs, we sketch an underpinning pathway as follows. The parametrically excited subharmonic tone $\frac{\omega_d}{2}$

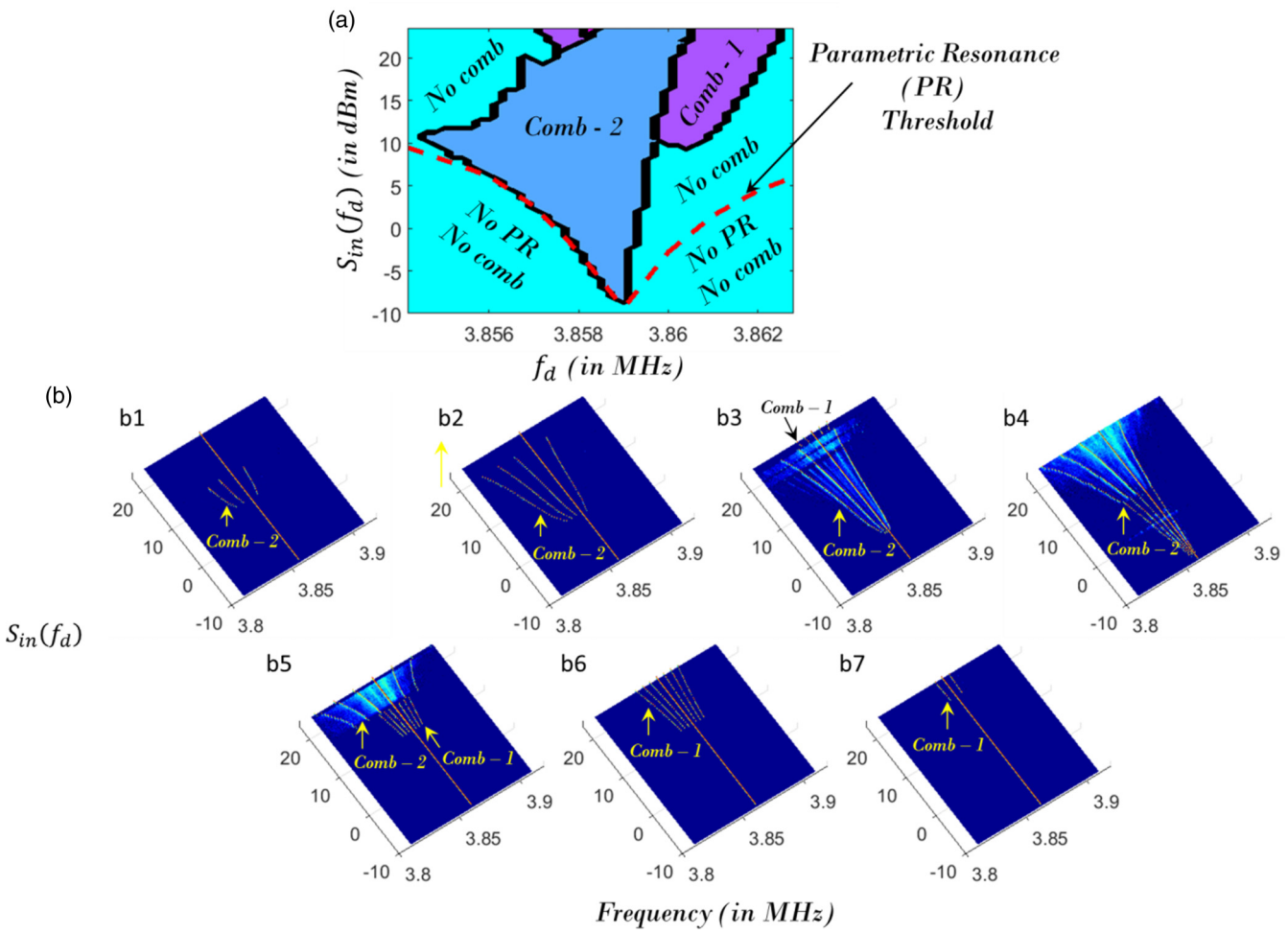


FIG. 3. Regimes of phononic frequency combs. (a) The regimes of phononic frequency combs for a range of drive frequencies $f_d = 3.8544-3.8626$ MHz and drive power levels $S_{\text{in}} = -10$ to 23.5 dBm; (b): (b1)–(b7) The drive power level dependent output spectra $S_{\text{out}}$ for different drive frequencies $f_d = 3.856$, 3.857, 3.858, 3.859, 3.86, 3.861, and 3.862 MHz.

may excite $\omega_2$ through parametric back action. This back action is related to the dynamical coupling of the driven and self-excited modes. While such parametric back action can be evidenced only through the differing drive level dependences of driven and self-excited tones (cf. Fig. 2 of Ref. [8]); a direct observation of such an effect can be obtained through the excitation of frequency combs. Also, the frequencies $\omega_1$ or $\omega_2$ may also be drive power level dependent. Hence, we replace $\omega_1$ and $\omega_2$ by the re-normalized frequencies $\tilde{\omega}_1$ and $\tilde{\omega}_2$, respectively. We have thus qualitatively argued the possibility for the multiple classes of frequency combs in the context of the Eq. (2). Now, we experimentally map the regimes specific to these classes of frequency combs at different drive conditions.

For a drive frequency $f_d = \frac{\omega_d}{2\pi} = 3.86$ MHz, we had already mapped the nature of resonances for a range of power levels $-10$ to 23.5 dBm [Fig. 1(b)]. This revealed the transition from $\omega_d$ (no parametric resonance; no frequency comb) to $\omega_d$ and $\frac{\omega_d}{2}$ (no frequency comb) to $\omega_d \pm n(\omega_d - \tilde{\omega}_1)$; $\frac{\omega_d}{2} \pm n(\omega_d - \tilde{\omega}_1)$ (frequency comb 1) to $\omega_d \pm n(\omega_d - \tilde{\omega}_2)$; $\frac{\tilde{\omega}_2}{2} \pm n(\omega_d - \tilde{\omega}_2)$ (frequency comb 2). Now, we chart such regimes for different drive frequencies and power levels. As shown in Fig. 3, the regimes specific to the excitation of frequency comb 1 and 2 are nonstandard and are not merely characterized by a mere parametric resonance threshold. For instance, for the drive frequencies 3.86 MHz $< f_d <$ 3.863 MHz, the comb and parametric excitation thresholds are not the same (Fig. 3). Hence, regimes exist in which the parametric excitation takes place without the frequency comb formation. However, the most intriguing feature of Fig. 3 is the fact that the frequency comb 2 transitions into parametric resonance at high-drive levels for 3.855 MHz $< f_d <$ 3.857 MHz [Figs. 3(b1) and 3(b2)]. Furthermore, in previous observations of Refs. [1] and [35], the frequency combs were observed only outside the dispersion band. In contrast, the current experiments show the possibility for comb generation even within the dispersion band. Despite these variations, in general, the drive conditions for the excitation of frequency combs 1 and 2 are well bounded.

As briefly mentioned before, the frequency comb spacing is drive level dependent, and Fig. 4 presents this dependence. While the spacing increases with the drive power level, it is nearly constant with the drive frequency at a specific drive power level [Figs. 4(a) and 4(c)]. This is similar to the case presented in the previous work (cf. Fig. 3 in Ref. [1]). However, the difference is the nature of drive level dependence. In

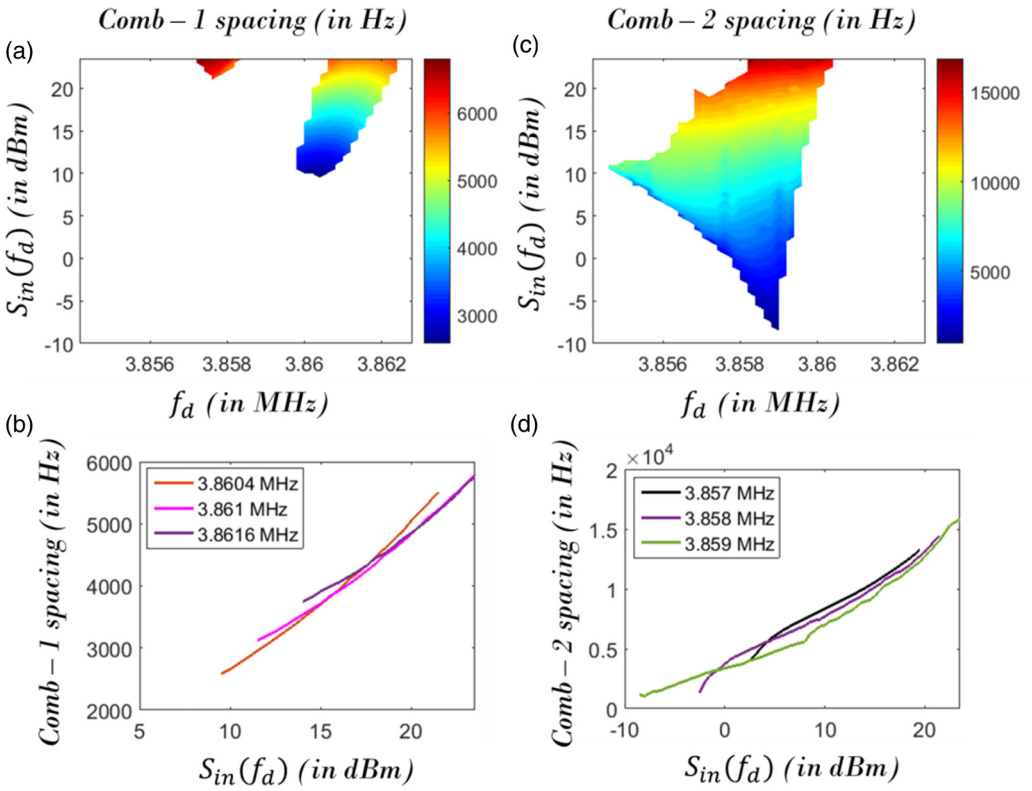


FIG. 4. Spacing of phononic frequency combs. (a), (c) The spacing of frequency combs 1 and 2 for a range of drive frequencies $f_d =$ 3.8544 to 3.8626 MHz and drive power levels $S_{\text{in}} = -10$ to 23.5 dBm. The absence of color indicates the absence of the respective frequency comb. (b) The drive power level dependent spacing of frequency comb 1 for different drive frequencies $f_d = 3.8604$, 3.861, and 3.8616 MHz. (d) The drive power level dependent spacing of frequency comb 2 for different drive frequencies $f_d = 3.857$, 3.858, and 3.859 MHz.

contrast to the linear increase with the drive power level (cf. Fig. 3 in Ref. [1]), the dependences in the current experiments are quadratic [Fig. 4(b)] and cubic [Fig. 4(d)]. While the linear dependence of resonance frequency with drive level can be related to the cubic nonlinearity inherent to Duffing oscillation, the quadrative and cubic dependences [Figs. 4(b) and 4(d)] may emerge from higher order nonlinearities for instance, fifth-order [38], or a combination of high-order nonlinearities. While the modulation of resonant responses via high-order nonlinearities [38] can be interesting in its own, the interplay of such effects with the frequency comb generation process, as in Fig. 3 in Ref. [1] and Figs. 4(b) and 4(d), provides avenues for further research studies on the underlying dynamics.

In summary, the excitation of two coupled frequency combs using two-mode parametric three-wave mixing has been observed in a specific system of two mechanically coupled micromechanical resonators. The fundamental nature of the component frequency combs is different. While the tone at half the drive frequency $\frac{f_d}{2}$ is observed in one frequency comb, it is absent in the other. Also, the spacing and its nonlinear drive level dependence are different for such frequency combs. Mutually exclusive well-bounded regimes for each component frequency combs also exist, and such regimes are not merely described by the parametric resonance threshold. In the future, multiple experiments with the advanced designs of micromechanical resonator are warranted to attain new insights into the nonlinear physics and also to arrive at the rigorous analytical descriptions modeling the precise nature of frequency combs. Such studies will also enable practical applications, for example, the use of phononic frequency combs for resonant frequency tracking [39].

Funding from the Cambridge Trusts is gratefully acknowledged.

[1] A. Ganesan, C. Do, and A. Seshia, Phononic Frequency Comb Via Intrinsic Three-Wave Mixing, Phys. Rev. Lett. **118**, 033903 (2017).

[2] L. S. Cao, D. X. Qi, R. W. Peng, M. Wang, and P. Schmelcher, Phononic Frequency Combs through Nonlinear Resonances, Phys. Rev. Lett. **112**, 075505 (2014).

[3] K. L. Turner, S. A. Miller, P. G. Hartwell, and N. C. MacDonald, Five parametric resonances in a microelectromechanical system, Nature **396**, 149 (1998).

[4] D. W. Carr, S. Evoy, L. Sekaric, H. G. Craighead, and J. M. Parpia, Parametric amplification in a torsional microresonator, Appl. Phys. Lett. **77**, 1545 (2000).

[5] R. B. Karabalin, X. L. Feng, and M. L. Roukes, Parametric nanomechanical amplification at very high frequency, Nano Lett. **9**, 3116 (2009).

[6] A. Eichler, J. Chaste, J. Moser, and A. Bachtold, Parametric amplification and self-oscillation in a nanotube mechanical resonator, Nano Lett. **11**, 2699 (2011).

[7] Y. Jia, S. Du, and A. A. Seshia, Twenty-eight orders of parametric resonance in a microelectromechanical device for multiband vibration energy harvesting, Sci. Rep., **6**, 30167 (2017).

[8] A. Ganesan, C. Do, and A. Seshia, Observation of three-mode parametric instability in a micromechanical resonator, Appl. Phys. Lett. **109**, 193501 (2016).

[9] A. Ganesan, C. Do, and A. Seshia, Excitation of multiple 2-mode parametric resonances by a single driven mode, Europhys. Lett. **119**, 10002 (2017).

[10] M. J. Seitner, M. Abdi, A. Ridolfo, M. J. Hartmann, and E. M. Weig, Parametric Oscillation, Frequency Mixing, and Injection Locking of Strongly Coupled Nanomechanical Resonator Modes, Phys. Rev. Lett. **118**, 254301 (2017).

[11] A. Ganesan, C. Do, and A. Seshia, Towards N-mode parametric electromechanical resonances, arXiv:1708.01660.

[12] K. Wang, A.-C. Wong, and C.-C. Nguyen, VHF free-free beam high-Q micromechanical resonators, J. Microelectromech. Syst. **9**, 347 (2000).

[13] C. L. Kirk and S. M. Wiedemann, Natural frequencies and mode shapes of a free-free beam with large end masses, J. Sound Vib. **254**, 939 (2002).

[14] A. T. Ferguson, L. Li, V. T. Nagaraj, B. Balachandran, B. Piekarski, and D. L. DeVoe, Modeling and design of composite free-free beam piezoelectric resonators, Sens. Actuators, A, **118**, 63 (2005).

[15] M. Palaniapan and L. Khine, Nonlinear behavior of SOI free-free micromechanical beam resonator, Sens. Actuators, A, **142**, 203 (2008).

[16] L. C. Shao, M. Palaniapan, W. W. Tan, and L. Khine, Nonlinearity in micromechanical free-free beam resonators: Modeling and experimental verification, J. Micromech. Microeng. **18**, 025017 (2008).

[17] K.-K. Hu and P. G. Kirmser, On the nonlinear vibrations of free-free beams, J. Appl. Mech. **38**, 461 (1971).

[18] R. B. Karabalin, M. C. Cross, and M. L. Roukes, Nonlinear dynamics and chaos in two coupled nanomechanical resonators, Phys. Rev. B **79**, 165309 (2009).

[19] S. Tallur and S. A. Bhave, Non-linear dynamics in optomechanical oscillators, *18th International Conference on Solid-State Sensors, Actuators and Microsystems (TRANSDUCERS)* (IEEE, Anchorage, AK, 2015), pp. 993–996.

[20] R. Lifshitz and M. C. Cross, Response of parametrically driven nonlinear coupled oscillators with application to micromechanical and nanomechanical resonator arrays, Phys. Rev. B **67**, 134302 (2003).

[21] E. Kenig, B. A. Malomed, M. C. Cross, and R. Lifshitz, Intrinsic localized modes in parametrically driven arrays of nonlinear resonators, Phys. Rev. E **80**, 046202 (2009).

[22] Y. Bromberg, M. C. Cross, and R. Lifshitz, Response of discrete nonlinear systems with many degrees of freedom, Phys. Rev. E **73**, 016214 (2006).

[23] G. Heinrich, M. Ludwig, J. Qian, B. Kubala, and F. Marquardt, Collective Dynamics in Optomechanical Arrays, Phys. Rev. Lett. **107**, 043603 (2011).

[24] U. Akram, W. Munro, K. Nemoto, and G. J. Milburn, Photon-phonon entanglement in coupled optomechanical arrays, Phys. Rev. A **86**, 042306 (2012).

[25] D. E. Chang, A. H. Safavi-Naeini, M. Hafezi, and O. Painter, Slowing and stopping light using an optomechanical crystal array, New J. Phys. **13**, 023003 (2011).

[26] J.-H. Gan, H. Xiong, L.-G. Si, X.-Y. Lu, and Y. Wu, Solitons in optomechanical arrays, Opt. Lett. **41**, 2676 (2016).

[27] E. Buks and M. L. Roukes, Electrically tunable collective response in a coupled micromechanical array, J. Microelectromech. Syst. **11**, 802 (2002).

[28] D. K. Agrawal, J. Woodhouse, and A. A. Seshia, Observation of Locked Phase Dynamics and Enhanced Frequency Stability in Synchronized Micromechanical Oscillators, Phys. Rev. Lett. **111**, 084101 (2013).

[29] P. Thiruvenkatanathan, J. Woodhouse, J. Yan, and A. A. Seshia, Manipulating vibration energy confinement in electrically coupled microelectromechanical resonator arrays, J. Microelectromech. Syst. **20**, 157 (2011).

[30] E. A. Martens, S. Thutupalli, A. Fourriere, and O. Hallatschek, Chimera states in mechanical oscillator networks, Proc. Natl. Acad. Sci. **110**, 10563 (2013).

[31] A. M. Hagerstrom, T. E. Murphy, R. Roy, P. Hovel, I. Omelchenko, and E. Scholl, Experimental observation of chimeras in coupled-map lattices, Nat. Phys. **8**, 658 (2012).

[32] D. M. Abrams and S. H. Strogatz, Chimera States for Coupled Oscillators, Phys. Rev. Lett. **93**, 174102 (2004).

[33] A. Ganesan, C. Do, and A. A. Seshia, Phononic four-wave mixing, arXiv:1610.08008.

[34] A. Ganesan, C. Do, and A. Seshia, Frequency transitions in phononic four-wave mixing, Appl. Phys. Lett. **111**, 064101 (2017).

[35] A. Ganesan, C. Do, and A. Seshia, Phononic frequency comb via three-mode parametric three-wave mixing, arXiv:1704.08008.

[36] A. Ganesan, C. Do, and A. Seshia, Observation of phononic frequency combs in a micromechanical resonator, in *Joint Conference of the European Frequency and Time Forum and IEEE International Frequency Control Symposium* (IEEE, Piscataway, NJ, 2017), pp. 148–152.

[37] See Supplemental Material at http://link.aps.org/supplemental/10.1103/PhysRevB.97.014302 for the response of two-coupled micromechanical resonators.

[38] M. Kumar, B. Choubey, and H. Bhaskaran, Nanomechanical resonators show higher order nonlinearity at room temperature, arXiv:1703.03094.

[39] A. Ganesan and A. Seshia, Tracking the resonant frequency of a micromechanical resonator using phononic frequency combs, arXiv:1710.07058.